

# A Rapid Microwave-Assisted Thermolysis Route to Highly Crystalline Carbon Nitrides for Efficient Hydrogen Generation

Yufei Guo, Jing Li, Yupeng Yuan,\* Lu Li, Mingyi Zhang, Chenyan Zhou, and Zhiqun Lin\*

**Abstract:** Highly crystalline graphitic carbon nitride ( $g\text{-C}_3\text{N}_4$ ) with decreased structural imperfections benefits from the suppression of electron–hole recombination, which enhances its hydrogen generation activity. However, producing such  $g\text{-C}_3\text{N}_4$  materials by conventional heating in an electric furnace has proven challenging. Herein, we report on the synthesis of high-quality  $g\text{-C}_3\text{N}_4$  with reduced structural defects by judiciously combining the implementation of melamine–cyanuric acid (MCA) supramolecular aggregates and microwave-assisted thermolysis. The  $g\text{-C}_3\text{N}_4$  material produced after optimizing the microwave reaction time can effectively generate  $\text{H}_2$  under visible-light irradiation. The highest  $\text{H}_2$  evolution rate achieved was  $40.5 \mu\text{mol h}^{-1}$ , which is two times higher than that of a  $g\text{-C}_3\text{N}_4$  sample prepared by thermal polycondensation of the same supramolecular aggregates in an electric furnace. The microwave-assisted thermolysis strategy is simple, rapid, and robust, thereby providing a promising route for the synthesis of high-efficiency  $g\text{-C}_3\text{N}_4$  photocatalysts.

Among various renewable energy sources, solar production of hydrogen ( $\text{H}_2$ ) fuel through photocatalytic water splitting is widely recognized as an ideal route to utilizing solar energy as both solar energy and water are highly abundant on Earth. Of the various materials that have been reported for active  $\text{H}_2$  generation under UV and visible-light irradiation,<sup>[1–8]</sup> graphitic carbon nitride ( $g\text{-C}_3\text{N}_4$ ) has garnered much attention as it is a highly active and stable photocatalyst for  $\text{H}_2$  generation upon exposure to visible light.<sup>[9–11]</sup> To date, several nitrogen-rich molecules, such as dicyandiamide, melamine, and urea, have been routinely used as precursors to produce  $g\text{-C}_3\text{N}_4$  at high temperatures (400–600 °C) in air or inert atmosphere.<sup>[9,10]</sup> Notably, these N-rich molecules can follow several reaction pathways with the formation of various intermediates during

the polycondensation of  $g\text{-C}_3\text{N}_4$ .<sup>[9,10]</sup> The characterization of  $g\text{-C}_3\text{N}_4$  reveals the presence of structural defects that are due to incompletely reacted intermediates, including amino and/or cyano groups.<sup>[12,13]</sup> The photocatalytic activity is sensitively affected by these structural defects because they can serve as charge trap sites in photocatalytic reactions. To address this issue, one strategy is to avoid the complicated reaction pathways, thus reducing the formation of intermediate products during the polycondensation into  $g\text{-C}_3\text{N}_4$ . The second strategy involves the preparation of highly crystalline  $g\text{-C}_3\text{N}_4$  to reduce the number of structural defects. It is noteworthy that the conventional synthetic approach, which involves heating in an electric furnace, cannot yield high-quality  $g\text{-C}_3\text{N}_4$  as noted above. Clearly, an effective synthetic strategy for the synthesis of highly crystalline  $g\text{-C}_3\text{N}_4$  is desirable yet challenging.

Compared with single-component N-rich precursors, the advantages of using supramolecular aggregates as starting materials for creating  $g\text{-C}_3\text{N}_4$  are twofold. First, the supramolecular aggregates possess a preorganized network that is structurally similar to the local arrangement in  $g\text{-C}_3\text{N}_4$  building blocks at the molecular level. Second, because of the hydrogen-bonded supramolecular structure, the supramolecular aggregates reduce the sublimation of the N-rich molecules (e.g., melamine) during polycondensation at elevated temperatures.<sup>[14,15]</sup> Consequently,  $g\text{-C}_3\text{N}_4$  samples obtained from supramolecular aggregates as starting precursors benefit from reduced structural defects and enhanced photocatalytic  $\text{H}_2$  generation.<sup>[14,15]</sup>

Herein, we report on a simple route for the synthesis of highly crystalline  $g\text{-C}_3\text{N}_4$  with a significantly reduced number of defects for high-efficiency  $\text{H}_2$  generation by judiciously combining the use of melamine–cyanuric acid supramolecular aggregates with rapid, microwave-assisted thermolysis. 1,3,5-Triazine-2,4,6-triol, a planar molecule with carbonyl groups at each vertex (compound **2** in Figure 1) was complexed with melamine (**1**) to produce hydrogen-bonded melamine–cyanuric acid (MCA) supramolecular aggregates (**3**). Intriguingly, the MCA supramolecular aggregates possess structural similarity to  $g\text{-C}_3\text{N}_4$  (**4**). They can thus be directly polymerized to yield  $g\text{-C}_3\text{N}_4$ , thereby eliminating the complicated reaction pathways involved in the formation of intermediates and producing  $g\text{-C}_3\text{N}_4$  with greatly reduced defects. Moreover, in sharp contrast to the conventional approach based on heating in an electric furnace, the microwave-assisted thermolysis approach enables the production of  $g\text{-C}_3\text{N}_4$  within minutes with greatly improved crystallinity owing to the strong rotation, friction, and collision of N-rich molecules under microwave irradiation.<sup>[16–18]</sup> The photocatalytic  $\text{H}_2$  generation rate of a  $g\text{-C}_3\text{N}_4$  sample thus obtained was two times higher

[\*] Y. Guo, J. Li, Dr. Y. Yuan, C. Zhou  
School of Chemistry and Chemical Engineering  
Anhui University  
Hefei 230601 (P. R. China)  
E-mail: yupengyuan@ahu.edu.cn

L. Li, Dr. M. Zhang  
School of Physics and Electronic Engineering  
Harbin Normal University  
Harbin 150025 (P. R. China)

Dr. Y. Yuan, Prof. Z. Lin  
School of Materials Science and Engineering  
Georgia Institute of Technology  
Atlanta, GA 30332 (USA)  
E-mail: zhiqun.lin@mse.gatech.edu

Supporting information for this article can be found under:  
<http://dx.doi.org/10.1002/anie.201608453>.

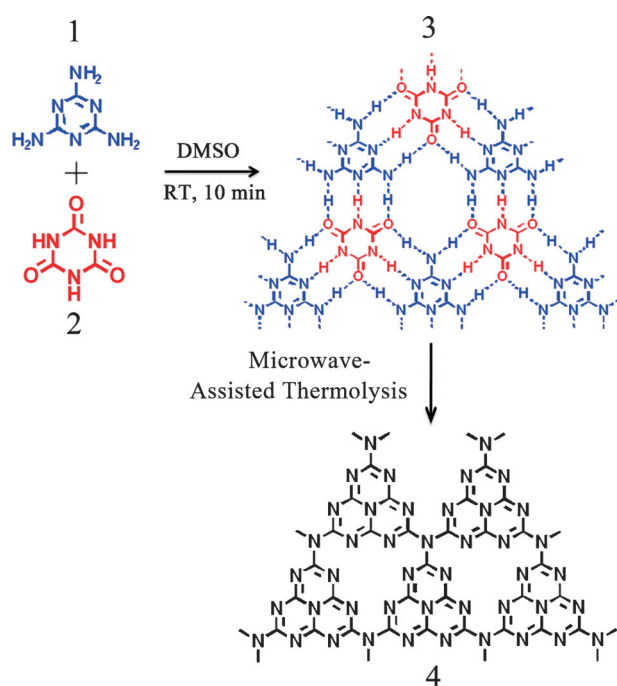


**Figure 1.** g-C<sub>3</sub>N<sub>4</sub> formation. Molecular structures of melamine (1), cyanuric acid (2), MCA supramolecular aggregates (3), and g-C<sub>3</sub>N<sub>4</sub> (4).

than that of a g-C<sub>3</sub>N<sub>4</sub> sample obtained by polymerizing MCA supramolecular aggregate in an electric furnace.

Specifically, MCA supramolecular aggregates (3) were precipitated from an equimolar mixture of melamine and cyanuric acid in dimethyl sulfoxide (DMSO). The MCA aggregates possess a spherical morphology with an average size of about 3  $\mu\text{m}$ , as shown by scanning electron microscopy (SEM; see the Supporting Information, Figure S1 a). Further analysis of the MCA spheres revealed that they are composed of closely assembled nanoparticles with an average size of 200 nm or smaller (Figure S1 b). The intense peaks at  $2\theta = 10^\circ$  and  $28^\circ$  in the XRD pattern were attributed to the periodic arrays of intraplanar stacking and interlayer aromatic stacking of MCA, respectively (Figure S2). Compared to g-C<sub>3</sub>N<sub>4</sub>, with peaks located at  $2\theta = 13^\circ$  and  $27.5^\circ$  as described below (Figure 2 a), the different peak positions of MCA ( $2\theta = 10^\circ$  and  $28^\circ$ ) may be due largely to the hydrogen-bonded network in MCA (3). Nonetheless, this XRD result further substantiated that the structure of MCA (3) bears a strong resemblance to g-C<sub>3</sub>N<sub>4</sub> (4).

Subsequently, the MCA supramolecular aggregates were thermalized for various periods of time using the microwave-assisted heating strategy (see the Experimental Section in the Supporting Information). CuO was used as the microwave absorber as it can intensely and effectively absorb microwaves to increase the temperature up to 1285 K in less than 7 min.<sup>[19]</sup> The resulting products were labeled CN<sub>*t*</sub>, where *t* is the microwave heating time in minutes. A control sample was also prepared by polymerizing the MCA supramolecular aggregates at 540 °C for 4 h in Ar atmosphere by conventional heating in an electric furnace (CN540). After 10 min polycondensation by microwave irradiation (yielding CN<sub>10</sub>), the products showed the yellow color typical of g-C<sub>3</sub>N<sub>4</sub>. The XRD

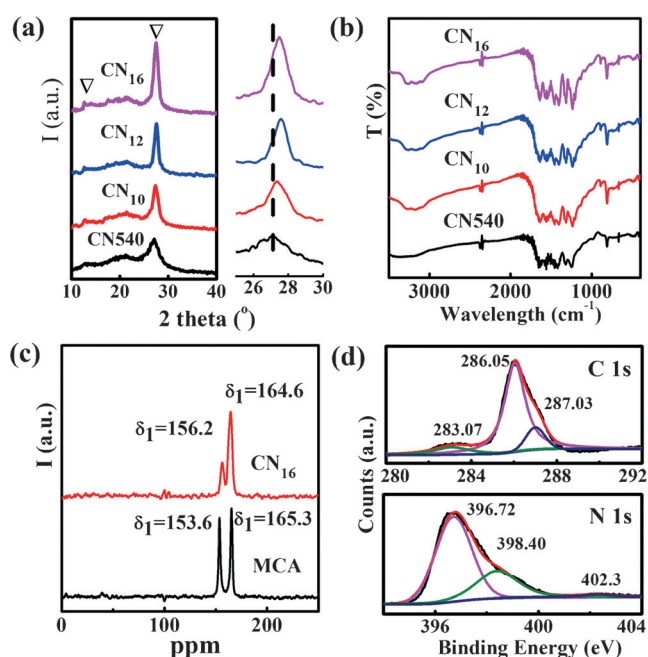


**Figure 2.** a) XRD patterns and b) FTIR spectra of CN<sub>*t*</sub> samples produced by microwave-assisted thermolysis of MCA precursors for 10, 12, and 16 min, respectively. The XRD pattern and FTIR spectrum of a reference sample (CN540) prepared by heating MCA precursors at 540 °C for 4 h are also provided for comparison. The right panel in (a) shows close-up XRD patterns of g-C<sub>3</sub>N<sub>4</sub> samples from  $2\theta = 25\text{--}30^\circ$ . c) <sup>13</sup>C MAS NMR spectra of MCA supramolecular aggregates and CN<sub>16</sub>. d) XPS spectra showing the binding energies of C 1s and N 1s for the CN<sub>16</sub> sample.

pattern of CN540 is essentially the same as that reported in the literature.<sup>[20]</sup> The two characteristic diffraction peaks at  $2\theta = 13^\circ$  and  $27.5^\circ$  ( $\nabla$ ) correspond to the periodic in-plane tri-s-triazine stacking and the interlayer structural aromatic packing, respectively (Figure 2 a).<sup>[16,21]</sup> The wide diffraction peak of the CN540 sample suggested that low-crystalline g-C<sub>3</sub>N<sub>4</sub> was produced by conventional heating. It is interesting to note that in spite of the different heating process with microwave-assisted heating of MCA for only 8 min, the CN<sub>8</sub> sample showed essentially the same XRD pattern as MCA with the emergence of a new diffraction peak at  $2\theta = 12^\circ$ , indicating the polymerization of melamine and cyanuric acid (Figure S2). Importantly, the CN<sub>10</sub> sample obtained after microwave-assisted thermolysis for 10 min displayed two distinct diffraction peaks at  $2\theta = 13^\circ$  and  $27.5^\circ$ , reflecting that g-C<sub>3</sub>N<sub>4</sub> had been formed after microwave-assisted heating for 10 min. Moreover, in comparison to the XRD pattern of the CN540 sample with a broad and weak peak at  $2\theta = 27.5^\circ$ , a relatively intense and narrower diffraction peak was observed in the CN<sub>10</sub> sample, indicating improved crystallinity. Prolonged reaction times of 12 and 16 min yielded g-C<sub>3</sub>N<sub>4</sub> (CN<sub>12</sub> and CN<sub>16</sub>) with progressively increasing diffraction peak intensities (Figure 2 a). We note that the  $27.5^\circ$  peak was shifted to a higher angle with increased reaction time (Figure 2 a, right), suggesting a decreased interlayer distance in the resulting CN<sub>12</sub> and CN<sub>16</sub> samples. Clearly, the increased XRD peak intensity and the decreased interlayer

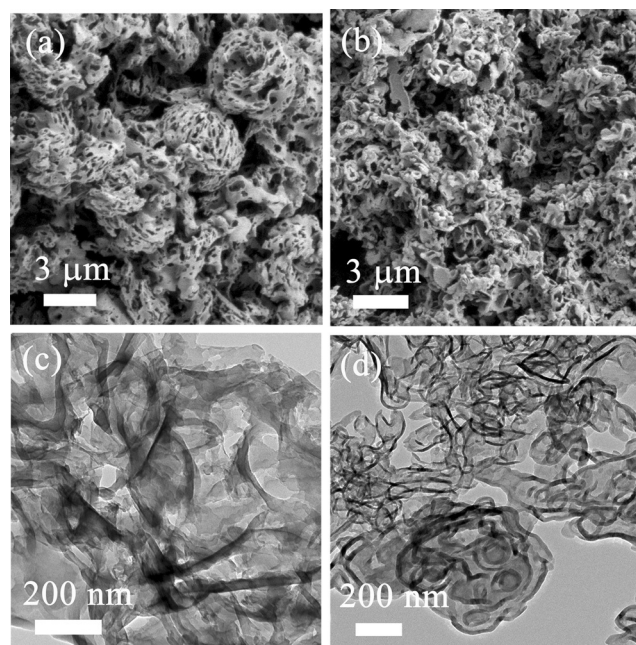
distance upon increasing the reaction time revealed that the polycondensation of the MCA precursors is enhanced by microwave-assisted thermolysis, resulting in highly crystalline  $g\text{-C}_3\text{N}_4$ .

FTIR measurements were performed to analyze the MCA polycondensation at different microwave reaction times (Figure 2b). The white  $\text{CN}_8$  sample gave rise to several bands at 3396, 3232, 1748, 1652, 1535, 1450, 1074, 1025, 910, 810, and 765  $\text{cm}^{-1}$ , corresponding to the MCA supramolecular aggregates (Figure S3). The increased intensity of these peaks in  $\text{CN}_8$  is indicative of the polycondensation of MCA; this is particularly true for the enhanced peak at 810  $\text{cm}^{-1}$ , a signature of the formation of tri-*s*-triazine (Figure S3).<sup>[14]</sup> In the  $\text{CN}_{10}$  sample, the characteristic peaks of the MCA precursors have disappeared, and new peaks have emerged at 810, 1240, 1318, 1411, 1460, 1568, and 1640  $\text{cm}^{-1}$ , which belong to the stretching vibrations of the CN heterocycles,<sup>[16]</sup> signifying the formation of tri-*s*-triazine.<sup>[16]</sup> The intensity of these peaks increased as the polycondensation reaction progressed (from  $\text{CN}_{10}$  to  $\text{CN}_{12}$  to  $\text{CN}_{16}$ ). The  $\text{NH}_2$  stretching vibration mode was observed at approximately 3200  $\text{cm}^{-1}$ .

The structure of the  $\text{CN}_{16}$  sample was further investigated by  $^{13}\text{C}$  MAS NMR spectroscopy (Figure 2c). The NMR spectrum showed two resolved resonances at  $\delta_1 = 156.2$  and  $\delta_2 = 164.6$  ppm, corresponding to the C(i) atoms in the  $\text{CN}_3$  groups and the C(e) atoms in  $\text{CN}_2(-\text{NH}_2)\text{C}$ , respectively (Figure S4). The  $^{13}\text{C}$  MAS NMR spectrum clearly corroborated the  $g\text{-C}_3\text{N}_4$  frameworks in  $\text{CN}_{16}$ .<sup>[16]</sup> Notably, the MCA supramolecular aggregates also displayed two resonances at  $\delta_1 = 153.6$  and  $\delta_2 = 165.3$  ppm, corroborating the structural similarity to  $\text{CN}_{16}$  (Figure 2c).

To further investigate the structural details of  $\text{CN}_{16}$ , samples were analyzed by X-ray photoelectron spectroscopy (XPS; Figure 2d). The XPS analysis confirmed the presence of carbon and nitrogen in  $\text{CN}_{16}$  (Figure S5). The O 1s peak is due to doped cyanuric acid (Figure S5). The carbon species with a binding energy of 286.05 eV arises from the  $\text{C}(\text{sp}^2)=\text{N}$  bonds in the *s*-triazine rings. The peak at 283.07 eV is a result of the graphitic carbon while the peak at 287.03 eV is due to C–O bonds. The N 1s binding energy can be deconvoluted into three peaks of 396.72, 398.40, and 402.32 eV (Figure 2d).<sup>[21,22]</sup> The strongest N 1s peak at 396.72 eV corresponds to  $\text{sp}^2$ -hybridized aromatic N atoms ( $\text{C}=\text{N}-\text{C}$ ) in the *s*-triazine rings. The N 1s peak at 398.4 eV is indicative of amino groups ( $\text{C}-\text{N}-\text{H}$ ), which is consistent with the FTIR measurements (Figure 2b). The weakest N 1s peak at 402.32 eV is due to the charging effect.<sup>[14,23]</sup>

Elemental analysis revealed the C/N molar ratios of  $\text{CN}_{540}$ ,  $\text{CN}_{10}$ ,  $\text{CN}_{12}$ , and  $\text{CN}_{16}$  to be 0.674, 0.671, 0.679, and 0.684, respectively. The nitrogen richness of the  $g\text{-C}_3\text{N}_4$  samples arises from the dangling  $\text{NH}_2$  groups in  $g\text{-C}_3\text{N}_4$ , as revealed by FTIR spectroscopy. Although the measured C/N molar ratios are lower than the theoretical ratio of 0.75 for  $g\text{-C}_3\text{N}_4$ , the progressively increasing C/N ratios clearly reflect the improved structural integrity of the CN<sub>*n*</sub> samples. We note that the suite of characterizations discussed above substantiate the rapid and effective formation of  $g\text{-C}_3\text{N}_4$  by microwave-assisted thermolysis of MCA supramolecular aggregates.



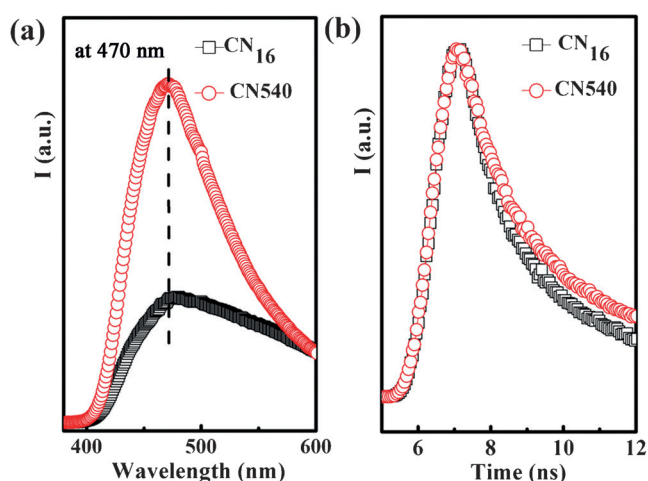
**Figure 3.** SEM images of a)  $\text{CN}_{540}$  and b)  $\text{CN}_{16}$ . TEM images of c)  $\text{CN}_{540}$  and d)  $\text{CN}_{16}$ . Whereas  $\text{CN}_{540}$  has a sphere-like morphology,  $\text{CN}_{16}$  has an irregular morphology resulting from the collapse of the MCA sphere precursors. Moreover, the  $\text{CN}_{16}$  nanosheets are thinner than those of  $\text{CN}_{540}$ .

Figure 3 shows representative SEM and TEM images of  $\text{CN}_{16}$  and  $\text{CN}_{540}$  samples. The  $\text{CN}_{540}$  sample displayed a loose and porous sphere-like morphology with an average sphere size of about 4  $\mu\text{m}$  (Figure 3a). The overall appearance of  $\text{CN}_{540}$  resembles that of the MCA precursors. Interestingly, the  $\text{CN}_{540}$  spheres are composed of velvet-like nanosheets with a thickness of less than 30 nm (Figure 3c). In contrast, the  $\text{CN}_{16}$  sample exhibited an irregular morphology. Obviously, the MCA spheres shown in Figure S1 had completely collapsed after microwave-assisted heating for 16 min (Figure 3b), which is due to the large amount of gases, such as  $\text{NH}_3$ , spontaneously generated during the polycondensation of the MCA supramolecular aggregates. The quick escape of gases led to the formation of highly fluffy and porous structures. The  $g\text{-C}_3\text{N}_4$  nanosheets produced by microwave-assisted heating were also further visualized by TEM (Figure 3d).

UV/Vis absorption spectra of  $g\text{-C}_3\text{N}_4$  samples produced by microwave-assisted heating for different periods of time ( $\text{CN}_{10}$ ,  $\text{CN}_{12}$ , and  $\text{CN}_{16}$ ) and the control example ( $\text{CN}_{540}$ ) are shown in Figure S6. The band gap of the  $\text{CN}_{16}$  sample was estimated to be 2.7 eV based on the onset of the absorption edge.<sup>[16]</sup> It is noticeable that the intensity of the absorption in the visible region increased with the microwave reaction time.

The effective transfer of photogenerated charge carriers depends sensitively on the trap sites in the semiconductor, which are closely related to the structural defects of the material. In this context, the steady-state photoluminescence (PL) upon excitation at 350 nm was measured in order to study the charge recombination in  $g\text{-C}_3\text{N}_4$ . As shown in Figure 4a, the  $\text{CN}_{540}$  sample gave rise to a strong emission





**Figure 4.** a) Steady-state PL spectra and b) time-resolved PL spectra of CN<sub>16</sub> and CN540 samples. The quenching of the PL intensity in the CN<sub>16</sub> sample signifies the reduced structural defects within the framework. In addition, the shorter lifetime in CN<sub>16</sub> indicates that charge transfer is more rapid than in the CN540 sample.

peak centered at 470 nm. In contrast, a significantly smaller emission peak was observed for CN<sub>16</sub>, suggesting decreased recombination of photogenerated electron–hole pairs. This observation further supported the reduced structural defects in the CN<sub>16</sub> sample as defects commonly serve as electron–hole recombination centers. More importantly, the improved crystallinity of the CN<sub>i</sub> samples (Figure 2a) resulted in rapid charge transfer in the CN<sub>16</sub> sample compared to CN540, as confirmed by time-resolved PL spectroscopy measurements (Figure 4b). The average PL lifetimes of CN540 and CN<sub>16</sub> were 3.96 and 2.79 ns, respectively. The shorter lifetime of the charge carriers in CN<sub>16</sub> signifies the rapid transfer of photogenerated electron–hole pairs involved in the redox reaction for CN<sub>16</sub>, thereby potentially promoting the photocatalytic H<sub>2</sub> production.<sup>[24]</sup>

Visible-light-induced photocatalytic H<sub>2</sub> generation was then attempted by capitalizing on the produced g-C<sub>3</sub>N<sub>4</sub> samples (20 mg) in the presence of triethanolamine (TEOA) as the sacrificial electron donor. Pt (0.5 wt %) was photoloaded in situ onto all g-C<sub>3</sub>N<sub>4</sub> samples as a co-catalyst to boost H<sub>2</sub> generation. Control experiments showed that no H<sub>2</sub> generation occurred in the absence of either photocatalyst or light irradiation, confirming that H<sub>2</sub> generation requires both light irradiation and a g-C<sub>3</sub>N<sub>4</sub> photocatalyst. The photocatalytic H<sub>2</sub> generation rate of CN<sub>10</sub> was determined to be 19.8 μmol h<sup>-1</sup>, which is comparable to that of a CN540 sample (22.4 μmol h<sup>-1</sup>; Figure 5a). Notably, the g-C<sub>3</sub>N<sub>4</sub> sample prepared by polycondensation of melamine alone at 540 °C for 4 h in Ar in an electric furnace (M540) only showed a H<sub>2</sub> generation rate of 6 μmol h<sup>-1</sup> under the same experimental conditions. This result clearly demonstrates the advantage of using the MCA supramolecular aggregates as precursors instead of melamine alone to create g-C<sub>3</sub>N<sub>4</sub>. The photocatalytic H<sub>2</sub> generation activity was even higher with the CN<sub>i</sub> samples with increased microwave reaction times. The highest H<sub>2</sub> evolution rate of 40.5 μmol h<sup>-1</sup> was achieved with the CN<sub>16</sub> sample; this value is nearly two times larger than that of the

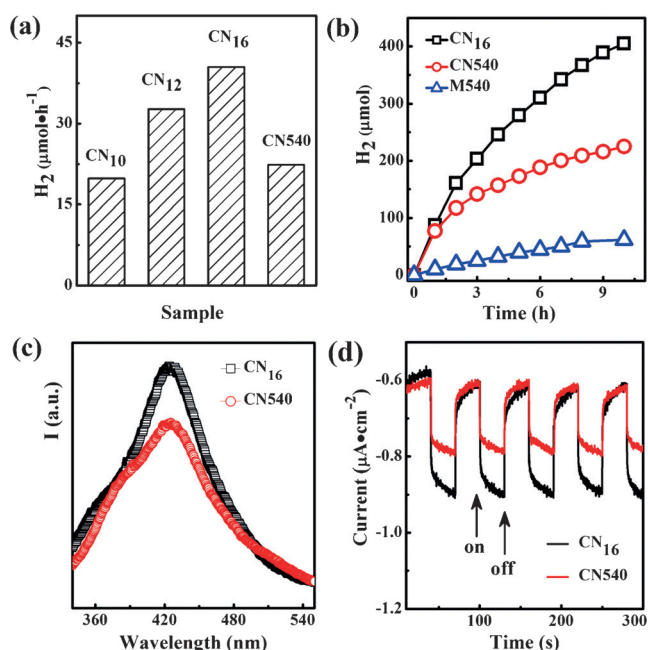


**Figure 5.** a) Photocatalytic H<sub>2</sub> generation rates of CN<sub>i</sub> and CN540 samples. b) H<sub>2</sub> generation with CN<sub>16</sub>, CN540, and M540 samples as a function of time. The M540 sample was prepared by polycondensation of melamine alone at 540 °C for 4 h in Ar. c) Photoluminescence spectra of TAOH formed by the reaction of TA with ·OH radicals generated from CN<sub>16</sub> and CN540 samples under visible-light irradiation for 10 min. d) Transient photocurrent response of ITO/CN<sub>16</sub> and ITO/CN540 at -1.0 V vs. Ag/AgCl in 0.5 M Na<sub>2</sub>SO<sub>4</sub> exposed to visible light (λ ≥ 420 nm, 300 W Xe lamp).

CN540 sample and more than six times larger than that of the M540 sample. The H<sub>2</sub> evolution rate of 40.5 μmol h<sup>-1</sup> is relatively high as the specific surface area of CN<sub>16</sub> (45.3 m<sup>2</sup> g<sup>-1</sup>) is 1.5 times smaller than that of CN540 (68.3 m<sup>2</sup> g<sup>-1</sup>), which further substantiates the effectiveness of the present microwave-assisted thermolysis strategy for high-quality g-C<sub>3</sub>N<sub>4</sub> production. Interestingly, the initial H<sub>2</sub> generation rates of CN<sub>16</sub> and CN540 were essentially the same during the first hour (Figure 5b). As the microwave reaction time was increased, the H<sub>2</sub> generation rate was comparatively reduced for the CN540 sample, revealing the enhanced stability of the CN<sub>16</sub> sample for photocatalytic H<sub>2</sub> generation, which is a direct consequence of the improved crystallinity of the CN<sub>i</sub> samples as determined by XRD (Figure 2a).

As noted above, the enhanced photocatalytic H<sub>2</sub> production can be ascribed to the reduced structural defects and the improved crystallinity of the CN<sub>i</sub> samples and thus the decreased number of trap sites in g-C<sub>3</sub>N<sub>4</sub> for efficient separation of photogenerated electron–hole pairs. To confirm the effectiveness of the charge separation, we carried out ·OH radical concentration measurements. As the ·OH radicals can oxidize terephthalic acid (TA) to 2-hydroxyterephthalic acid (TAOH), which has a strong emission peak at 426 nm,<sup>[25,26]</sup> the fluorescence intensity of TAOH can be used to monitor the charge separation efficiency. Compared to the CN540 sample, the higher fluorescence intensity of TAOH (Figure 5c) in the CN<sub>16</sub> sample revealed that more holes in the excited CN<sub>16</sub> sample are involved in the oxidation reaction of TA than in

the CN540 sample, indicating the more effective charge separation in CN<sub>16</sub> compared to CN540.

We measured the transient photocurrent in CN<sub>16</sub> and CN540 samples to further evaluate the efficient separation of electron-hole pairs in the CN<sub>16</sub> sample (Figure 5d with the dark current subtracted). The photocurrent responses were prompt and reproducible during the on/off cycles of visible-light excitation. Despite the relatively small value, the photocurrent generated in the CN<sub>16</sub> sample was still comparatively large compared to that in CN540, clearly confirming the effective separation of photoinduced electrons and holes in CN<sub>16</sub> compared to CN540.

In summary, we have developed a rapid and effective strategy that is based on the microwave-assisted thermolysis of MCA supramolecular aggregates to synthesize highly crystalline g-C<sub>3</sub>N<sub>4</sub> with reduced structural defects and enhanced photocatalytic H<sub>2</sub> generation activity under visible-light irradiation. The efficient separation of photogenerated electrons and holes in highly crystalline g-C<sub>3</sub>N<sub>4</sub> accounted for the enhanced H<sub>2</sub> generation. This inexpensive microwave-assisted strategy for the thermolysis of precursors and supramolecular aggregates may open possibilities for the targeted design of a broad range of high-efficiency photocatalysts with potential applications in water splitting, photocatalytic degradation of organic pollutants, and photoelectrochemical anticorrosion.

### Acknowledgements

This work was financially supported by the National Natural Science Foundation of China (51572003), Anhui Provincial Natural Science Foundation (1508085ME105, 1408085MB22), the Project sponsored by SRF for ROCS, SEM, and Technology Foundation for Selected Overseas Chinese Scholar, Ministry of Personnel of China.

**Keywords:** graphitic carbon nitride · microwave-assisted thermolysis · photocatalysis · supramolecular aggregates · water splitting

**How to cite:** *Angew. Chem. Int. Ed.* **2016**, *55*, 14693–14697  
*Angew. Chem.* **2016**, *128*, 14913–14917

[1] A. Fujishima, K. Honda, *Nature* **1972**, *238*, 37–38.

- [2] A. Kudo, Y. Miseki, *Chem. Soc. Rev.* **2009**, *38*, 253–278.  
[3] X. Chen, S. Shen, L. Guo, S. Mao, *Chem. Rev.* **2010**, *110*, 6503–6570.  
[4] Y. Yuan, L. Ruan, J. Barber, S. C. J. Loo, C. Xue, *Energy Environ. Sci.* **2014**, *7*, 3934–3951.  
[5] X. Li, J. Yu, M. Jaroniec, *Chem. Soc. Rev.* **2016**, *45*, 2603–2636.  
[6] J. Hu, A. Liu, H. Jin, D. Ma, D. Yin, P. Ling, S. Wang, Z. Lin, J. Wang, *J. Am. Chem. Soc.* **2015**, *137*, 11004–11010.  
[7] M. Ye, J. Gong, Y. Lai, C. Lin, Z. Lin, *J. Am. Chem. Soc.* **2012**, *134*, 15720–15723.  
[8] B. Han, Y. H. Hu, *J. Phys. Chem. C* **2015**, *119*, 18927–18934.  
[9] S. Cao, J. Low, J. Yu, M. Jaroniec, *Adv. Mater.* **2015**, *27*, 2150–2176.  
[10] S. Ye, R. Wang, M. Wu, Y. Yuan, *Appl. Surf. Sci.* **2015**, *358*, 15–27.  
[11] Y. Zheng, L. Lin, B. Wang, X. Wang, *Angew. Chem. Int. Ed.* **2015**, *54*, 12868–12884; *Angew. Chem.* **2015**, *127*, 13060–13077.  
[12] Z. Lin, X. Wang, *Angew. Chem. Int. Ed.* **2013**, *52*, 1735–1738; *Angew. Chem.* **2013**, *125*, 1779–1782.  
[13] M. K. Bhunia, K. Yamauchi, K. Takanabe, *Angew. Chem. Int. Ed.* **2014**, *53*, 11001–11005; *Angew. Chem.* **2014**, *126*, 11181–11185.  
[14] Y. Jun, E. Z. Lee, X. Wang, W. H. Hong, G. D. Stucky, A. Thomas, *Adv. Funct. Mater.* **2013**, *23*, 3661–3667.  
[15] M. Shalom, S. Inal, C. Fettekenhauer, D. Neher, M. Antonietti, *J. Am. Chem. Soc.* **2013**, *135*, 7118–7121.  
[16] Y. Yuan, L. Yin, S. Cao, L. Gu, G. Xu, P. Du, H. Chai, Y. Liao, C. Xue, *Green Chem.* **2014**, *16*, 4663–4668.  
[17] L. Lin, P. Ye, C. Cao, Q. Jin, G. Xu, Y. Shen, Y. Yuan, *J. Mater. Chem. A* **2015**, *3*, 10205–10208.  
[18] R. Hoogenboom, U. S. Schubert, *Macromol. Rapid Commun.* **2007**, *28*, 368–386.  
[19] K. J. Rao, B. Vaidhyanathan, M. Ganguli, P. A. Ramakrishnan, *Chem. Mater.* **1999**, *11*, 882–895.  
[20] X. Wang, K. Maeda, A. Thomas, K. Takanabe, G. Xin, J. M. Carlsson, K. Domen, M. Antonietti, *Nat. Mater.* **2009**, *8*, 76–80.  
[21] Y. Yuan, W. Xu, L. Yin, S. Cao, Y. Liao, Y. Tng, C. Xue, *Int. J. Hydrogen Energy* **2013**, *38*, 13159–13163.  
[22] Y. Cui, Z. Ding, X. Fu, X. Wang, *Angew. Chem. Int. Ed.* **2012**, *51*, 11814–11818; *Angew. Chem.* **2012**, *124*, 11984–11988.  
[23] J. Liu, T. Zhang, Z. Wang, G. Dawson, W. Chen, *J. Mater. Chem.* **2011**, *21*, 14398–14401.  
[24] J. Lee, H. S. Shim, M. Lee, J. K. Song, D. Lee, *J. Phys. Chem. Lett.* **2011**, *2*, 2840–2845.  
[25] J. Huang, K. Ding, X. Wang, X. Fu, *Langmuir* **2009**, *25*, 8313–8319.  
[26] G. Liu, P. Niu, L. Yin, H. Cheng, *J. Am. Chem. Soc.* **2012**, *134*, 9070–9073.

Received: August 29, 2016

Published online: October 6, 2016